Inorganic Chemistry

Article

pubs.acs.org/IC

Charge Delocalization of 1,4-Benzenedicyclometalated Ruthenium: A Comparison between Tris-bidentate and Bis-tridentate Complexes

Long-Zhen Sui,[†,‡,§] Wen-Wen Yang,[†,§] Chang-Jiang Yao,[†] Hai-Yan Xie,[‡] and Yu-Wu Zhong*[,†]

[†]Beijing National Laboratory for Molecular Sciences, CAS Key Laboratory of Photochemistry, Institute of Chemistry, Chinese Academy of Sciences, Beijing 100190, People's Republic of China

[‡]School of Life Science and Technology, Beijing Institute of Technology, Beijing 100081, People's Republic of China

Supporting Information

ABSTRACT: A dimetallic biscyclometalated ruthenium complex, $[(bpy)_2Ru(dpb)Ru(bpy)_2]^{2+}$ (bpy = 2,2′-bipyridine; dpb = 1,4-di-2-pyridylbenzene), with a tris-bidentate coordination mode has been prepared. The electronic properties of this complex were studied by electrochemical and spectroscopic analysis and DFT/TDDFT calculations on both rac and meso isomers. Complex $[(bpy)_2Ru(dpb)Ru(bpy)_2]^{2+}$ has a similar 1,4-benzenedicyclometalated ruthenium (Ru−phenyl−Ru) structural component with a previously reported bis-tridentate complex, $[(tpy)Ru(tpb)Ru(tpy)]^{2+}$ (tpy = 2,2′;6′,2″-terpyridine; tpb = 1,2,4,5-tetra-2-pyridylbenzene). The charge delocalizations of these complexes across the Ru−phenyl−Ru array were investigated and compared by studying the corresponding one-electron-oxidized species, generated by chemical oxidation or electrochemical electrolysis, with DFT/TDDFT calculations and spectroscopic and EPR analysis. These studies indicate that both $[(bpy)_2Ru(dpb)Ru(bpy)_2]^{3+}$ and $[(tpy)Ru(tpb)Ru(tpy)]^{3+}$ are fully delocalized systems. However, the coordination mode of the metal component plays an important role in influencing their electronic properties.

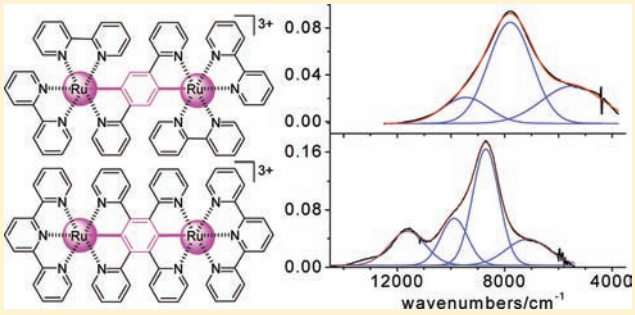

INTRODUCTION

The studies of organometallic complexes with a covalent bond between the ligand and metal center have been the focus of many research activities.[1] Organic ligands in these complexes are electron-rich, and some representative examples are phenyl anion,[1] phenylacetylide,[2] phenylvinylene anion,[3] and anionic nitrogen donors.[4] As for the metal components, ruthenium,[5] iron,[6] platinum,[7] and iridium[8] are most employed partly because these metals form stable complexes with anionic ligands. These complexes display appealing electronic properties and are identified as promising materials for applications in organic catalysis,[9] molecular electronics,[10] nonlinear optics,[11] and dye-sensitized solar cells.[12] One particularly interesting property of these complexes is that the extensive orbital overlap between the metal center and ligand complicates the redox process. In other words, these ligands are redox-noninnocent.[13] A specific redox process could be associated with the metal component or ligand unit or an admixture of them.

Dimetallic systems with the above-mentioned organometallic components with an anionic ligand are of special interest because of the redox noninnocent nature of the ligand. 1,4-Diethynylphenylene,[14] 1,4-divinylphenylene,[15] 4,4′-biphenyl dianion,[16] 2,7-pyrene dianion[17] and compounds with similar structural features are representative bridging ligands for the construction of these complexes. Assuming metal-confined redox behavior, the introduction of an anionic ligand strengthens the electron coupling between individual redox termini and affords mixed-valence systems with increasing electron delocalization. However, when the bridging ligand becomes redox-noninnocent, corresponding open-shell systems are no longer mixed-valent and classical Marcus−Hush theory[18] is not applicable. Elucidation of the charge delocalization degree in these systems needs detailed experimental studies in combination with computational calculations. We recently disclosed a dimetallic open-shell complex, $\mathbf{1}^{3+}$ (Figure 1), bridged by a redox-noninnocent 1,2,4,5-tetra-2-pyridylbenzene (tpb) ligand.[19] This complex was determined to be a fully electron-delocalized system across the central Ru−phenyl−Ru array. It displays multiple charge-transfer transitions in the near-IR (NIR) region. Herein, we report on a structurally related system $\mathbf{2}^{3+}$, where two ruthenium metals are connected with a 1,4-phenyl dianion bridge similar to that in $\mathbf{1}^{3+}$. However, the coordination environment of the metal was changed from bis-tridentate to tris-bidentate. The charge delocalizations of these two complexes across the central Ru−phenyl−Ru array were investigated and compared with multiple experimental and theoretical techniques. In addition, the studies of monometallic complexes $\mathbf{3}^{+}$ and $\mathbf{4}^{+}$ have also been included for comparison. It should be noted that different coordination modes of octahedral ruthenium complexes, namely, bis-tridentate or tris-bidentate, play an important role in determining their electronic structures and photophysical behaviors. For instance, the tris-bidentate complex $[Ru(bpy)_3]^{2+}$

Received: August 27, 2011
Published: January 11, 2012

   dx.doi.org/10.1021/ic202295b | Inorg. Chem. 2012, 51, 1590−1598

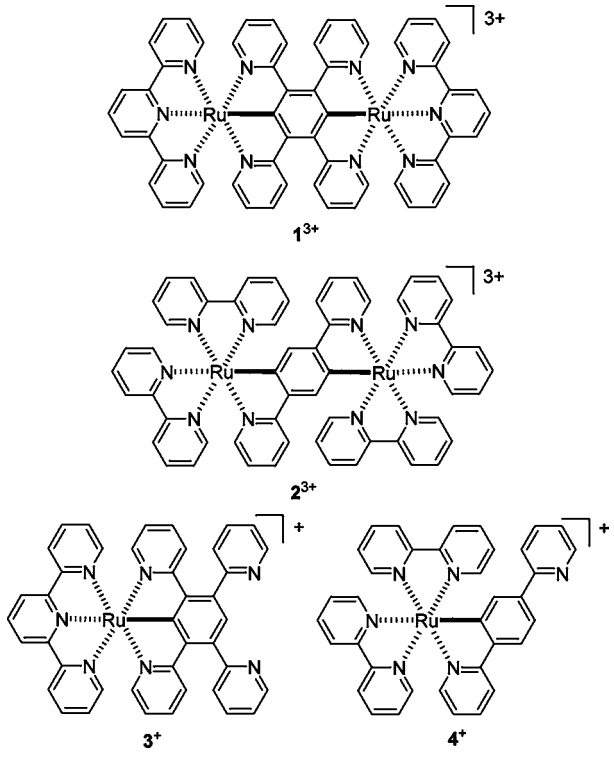

Figure 1. Cyclometalated complexes $\mathbf{1}^{3+}$, $\mathbf{2}^{3+}$, $\mathbf{3}^{+}$, and $\mathbf{4}^{+}$.

(bpy = 2,2′-bipyridine) is brightly emissive with a lifetime on the order of microseconds at room temperature.[20] On the other hand, the bis-tridentate complex $[Ru(tpy)_2]^{2+}$ (tpy = 2,2′:6′,2″-terpyridine) is virtually nonemissive at room temperature. However, it can be readily functionalized at the 4′ position of the tpy ligand and incorporated into supramolecular architectures with well-defined structures.[21] The effect of the coordination mode in cyclometalated ruthenium complexes with a covalent Ru−C bond has also been addressed recently.[22] More importantly, the coordination mode and even the stereochemistry in chiral systems can influence the nature of mixed-valent systems derived from polypyridine ligands.[23]

RESULTS AND DISCUSSION

Synthesis. The syntheses of tridentate complexes $\mathbf{1}^{2+}$ and $\mathbf{3}^{+}$ have been reported previously.[19] The syntheses of bidentate complexes $\mathbf{2}^{2+}$ and $\mathbf{4}^{+}$ started from the preparation of ligand **5**. As outlined in Scheme 1, the bridging ligand 1,4-di-2-pyridylbenzene (**5**, dpb) was obtained in 70% yield from the palladium-catalyzed Stille coupling between 1,4-dibromobenzene and 2-pyridyltributylstannane in the presence of anhydrous LiCl.[24] We note that **5** has previously been used to prepare a dinuclear cyclometalated iridium complex[25] and a diboron compound.[26] The reaction of **5** with 2 equiv of $Ru(bpy)_2Cl_2$ in the presence of AgOTf in a 1:1 mixed solvent of *N*,*N*-dimethylformamide (DMF) and ^{t}BuOH, followed by anion exchange with KPF_6 and chromatography using neutral alumina, afforded monometallic complex $\mathbf{4}^{+}$ and dimetallic complex $\mathbf{2}^{2+}$ in a yield of 40% and 18%, respectively. It must be stressed that the use of alumina is crucial for the successful isolation of the dimetallic complex $\mathbf{2}^{2+}$. We failed to purify $\mathbf{2}^{2+}$ in attempts using silica gel for flash column chromatography. However, this is not an issue for the monometallic complex $\mathbf{4}^{+}$ and the previously reported bis-tridentate dimetallic complex $\mathbf{1}^{2+}$. We found that a solution of $\mathbf{2}^{2+}$ in acetonitrile was contaminated by a small amount of the monometallic complex $\mathbf{4}^{+}$ after standing for several hours at room temperature, as monitored by thin-layer chromatography. However, this stability issue should not affect the following electrochemical and spectroscopic measurements. Complex $\mathbf{4}^{+}$ displays well-defined ^{1}H NMR peaks. However, the ^{1}H NMR spectrum of the dimetallic complex $\mathbf{2}^{2+}$ is rather complex and could not be assigned. It is very likely that it is composed of two diastereomers (rac and meso, Figure S1 in the Supporting Information) in a 1:1 ratio. We used this sample directly for the following electrochemical and spectroscopic measurements. The relative configurations of ruthenium components of two diastereomers are supposed to play a minor role in affecting their optoelectronic properties.[27] Although we have not been able to experimentally separate the rac and meso isomers of $\mathbf{2}^{2+}$, the following computational calculations have been performed on both isomers to estimate the differences in their electronic structures.

Scheme 1. Synthesis of 5, $\mathbf{4}^{+}$, and $\mathbf{2}^{2+}$

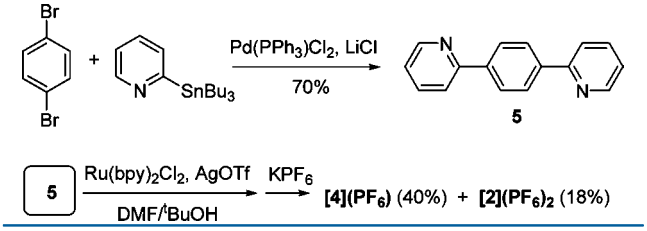

Electrochemical Studies and Density Functional Theory (DFT) Calculations. The electronic properties of the above-prepared samples were first studied by electrochemical analysis. Cyclic voltammetry (CV) profiles of $\mathbf{4}^{+}$ and $\mathbf{2}^{2+}$ are shown in Figure 2. Monometallic complex $\mathbf{4}^{+}$ displays an anodic redox couple at +0.55 V and two cathodic waves at −1.52 and −1.78 V vs Ag/AgCl, respectively. All of these peaks exhibit good chemical reversibility. In comparison, two consecutive anodic waves at +0.18 and +0.62 V are evident in the CV profile of the dimetallic complex $\mathbf{2}^{2+}$. The potential difference (ΔE) between two waves is 440 mV. This indicates a high thermodynamic stability of the in situ electrochemically generated open-shell complex $\mathbf{2}^{3+}$, with a comproportionation constant K_c of 2.87×10^7. We note that complex $\mathbf{1}^{2+}$ with two bis-tridentate ruthenium centers displays two similar anodic waves albeit at slightly negative potentials (+0.12 and +0.55 V vs Ag/AgCl, ΔE = 430 mV).[19] However, it should be kept in mind that the ΔE value should not be taken as a parameter for measuring the degree of electronic coupling between redox termini. A number of other factors, such as the electrostatic repulsion between like-charged metal centers, ion pairing with the electrolyte, and antiferromagnetic exchange, contribute to the degree of the ΔE value,[28] not to mention the different coordination modes in the cases of **1** and **2**. The cathodic scan of $\mathbf{2}^{2+}$ displays four closely spaced one-electron waves. Overall, anodic waves of $\mathbf{4}^{+}$ and $\mathbf{2}^{2+}$ are ascribed to the $Ru^{II/III}$ process, with appreciable contribution from oxidation of the cyclometalating ligand.[1,12,14−17] Cathodic waves are associated with the reduction of bpy ligands.

To assist in the determination of the electronic structures, DFT calculations were performed on complexes $\mathbf{4}^{+}$, *rac*-$\mathbf{2}^{2+}$, and *meso*-$\mathbf{2}^{2+}$ at the B3LYP/LANL2DZ/6-31G* level (see the Experimental Section for details). Their lowest unoccupied molecular orbital (LUMO) and highest occupied molecular orbital (HOMO) diagrams, together with those of $\mathbf{1}^{2+}$, are shown in Figure 3. More orbital graphics could be found in

dx.doi.org/10.1021/ic202295b | Inorg. Chem. 2012, 51, 1590−1598

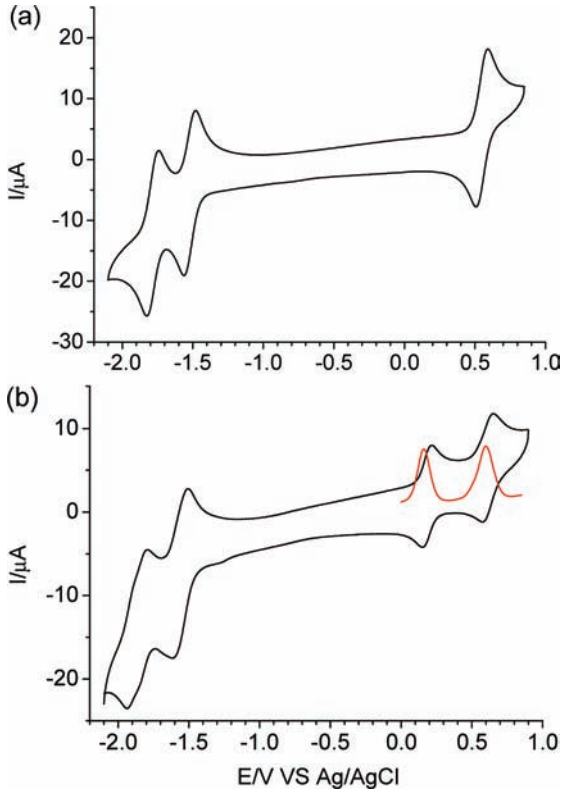

Figure 2. Cyclic voltammograms (black lines) of (a) 4^+ and (b) 2^{2+} in acetonitrile containing 0.1 M $^nBu_4NClO_4$ at a scan rate of 100 mV/s. The red lines are differential pulse voltammograms with a step potential of 5 mV and an amplitude of 50 mV. The working electrode is a glassy carbon, the counter electrode is a platinum wire, and the reference electrode is Ag/AgCl in saturated aqueous NaCl.

Figures S2 and S3 in the Supporting Information. All LUMOs of 4^+ and 2^{2+} are dominated by bpy ligands, which is in agreement with the assignment of their cathodic CV waves to the reduction of these ligands. The HOMO of 4^+ has major contribution from both the metal center and the cyclometalating phenyl ring, with Mulliken population values of 0.53 and 0.34, respectively. The electron densities of HOMOs of *rac*-2^{2+} and *meso*-2^{2+} distribute across the central Ru−phenyl−Ru array. The Mulliken populations of the two ruthenium centers and the cyclometalating phenyl fragment are 0.26, 0.23, and 0.33 for *rac*-2^{2+} and 0.29, 0.28, and 0.31 for *meso*-2^{2+}, respectively. We know from this calculation that *rac*-2^{2+} and *meso*-2^{2+} have similar albeit slightly different HOMO compositions. A comparison of the HOMO compositions for **1**−**4** is provided in Table 1. The extensive orbital overlap between metal centers and the cyclometalating phenyl ring has been found for the previously reported complex 1^{2+}.[19]

Table 1. Calculated Mulliken Populations of HOMOs of Complexes Studied

	Ru1	phenyl	Ru2
1^{2+}	0.25	0.29	0.25
rac-2^{2+}	0.26	0.33	0.23
meso-2^{2+}	0.29	0.31	0.28
3^+	0.48	0.34	
4^+	0.53	0.34	

The frontier orbital energy level alignment of complexes 1^{2+}, *rac*-2^{2+}, and *meso*-2^{2+} is shown in Figure 4. The calculation

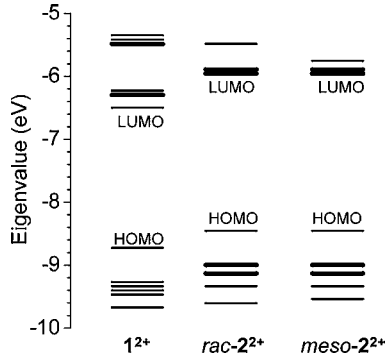

Figure 4. Frontier orbital energy level alignment of complexes 1^{2+}, *rac*-2^{2+}, and *meso*-2^{2+}.

methods for these complexes are identical, and they have the same charge (2+). Both HOMO and LUMO of 1^{2+} (−8.69 and −6.46 eV, respectively) are more stabilized than those of 2^{2+} (−8.40 eV and −5.97 eV, respectively). However, the difference of the LUMO levels between 1^{2+} and 2^{2+} (0.49 eV) is larger than that of the HOMO levels (0.29 eV). As a result, the calculated energy gap of 1^{2+} (2.23 eV) is narrower than that of 2^{2+} (2.43 eV for both isomers). The different energy levels of the calculated LUMOs of 1^{2+} and 2^{2+} can be easily understood. The LUMO of 1^{2+} is mainly associated with the bridging tpb ligand. However, the LUMO of 2^{2+} is mainly associated with the auxiliary bpy ligands. Consistent results were reflected from the above electrochemical analysis, which showed that the first reduction wave of 1^{2+} occurred at a less negative potential than that of 2^{2+} (−1.36 and −1.52 V vs

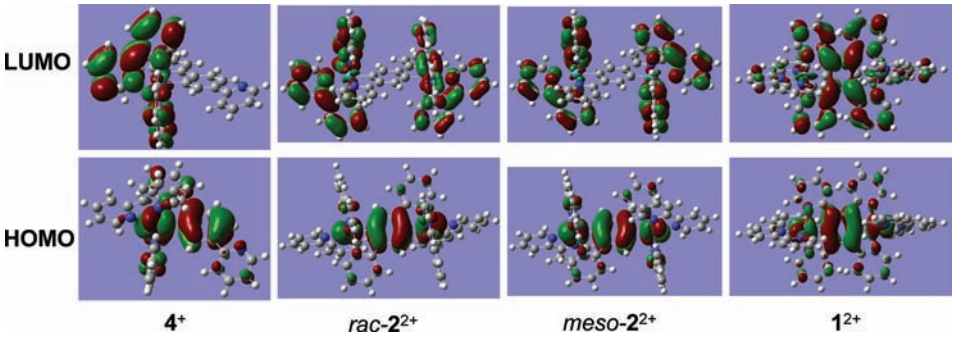

Figure 3. Isodensity plots of selected frontier orbitals for complexes 4^+, *rac*-2^{2+}, *meso*-2^{2+}, and 1^{2+}. All orbitals have been computed at an isovalue of 0.02.

dx.doi.org/10.1021/ic202295b | *Inorg. Chem.* 2012, 51, 1590−1598

Ag/AgCl). The slightly different HOMO levels of $\mathbf{1}^{2+}$ and $\mathbf{2}^{2+}$ could not be rationalized at this stage. As a matter of fact, the electrochemical results showed that the $Ru^{II/III}$ process of $\mathbf{1}^{2+}$ occurred at less positive potential than that of $\mathbf{2}^{2+}$ (+0.12 and +0.18 V vs Ag/AgCl), which is contradictory with the calculated results.

Electronic Absorption Spectra and Time-Dependent DFT (TDDFT) Calculations. The electronic absorption spectra of $\mathbf{4}^{+}$ and $\mathbf{2}^{2+}$ were recorded in acetonitrile and are shown in Figure 5, together with that of $\mathbf{1}^{2+}$. We previously found that

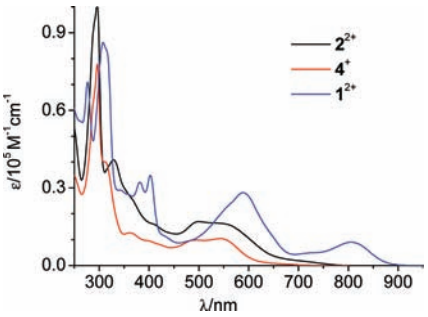

Figure 5. Electronic absorption spectra of complex $\mathbf{2}^{2+}$ (black line), $\mathbf{4}^{+}$ (red line), and $\mathbf{1}^{2+}$ (blue line) in acetonitrile.

the bis-tridentate complex $\mathbf{1}^{2+}$ exhibits a separate low-energy band at 805 nm in addition to the conventionally observed metal-to-ligand charge-transfer (MLCT) transitions in the visible region. However, in the case of the tris-bidentate complex $\mathbf{2}^{2+}$, no similar band is present. According to TDDFT calculations,[19] the peak at 805 nm of $\mathbf{1}^{2+}$ is of HOMO → LUMO origin. The HOMO compositions of $\mathbf{1}^{2+}$ and $\mathbf{2}^{2+}$ are quite similar, as described above. However, as has been described above, the LUMO of $\mathbf{1}^{2+}$ is mainly associated with the bridging tpb ligand and is more stabilized (−6.46 eV) than the auxiliary ligand bpy-dominated LUMO of $\mathbf{2}^{2+}$ (−5.97 eV for both *rac*-$\mathbf{2}^{2+}$ and *meso*-$\mathbf{2}^{2+}$). This difference is likely responsible for the absence of a low-energy absorption band for $\mathbf{2}^{2+}$. The absorption bands in the visible region for $\mathbf{4}^{+}$ and $\mathbf{2}^{2+}$ are ascribed to the MLCT transitions mixing with some contribution from the ligand-to-ligand charge-transfer (LLCT) transitions due to the significant involvement of the cyclometalating phenyl fragment in the HOMOs. In comparison, $\mathbf{2}^{2+}$ has higher molar absorptivity than $\mathbf{4}^{+}$ and its low-energy side extends into the NIR region. Bands in the ultraviolet region are attributed to the intraligand transitions from both bpy and dpb ligands. The observed red shift of the MLCT transitions and narrower optical energy gap of $\mathbf{1}^{2+}$, compared to those of $\mathbf{2}^{2+}$ and $\mathbf{4}^{+}$, agree well with the above electrochemical and calculation results.

In order to examine the possible difference of absorption between the rac and meso isomers of $\mathbf{2}^{2+}$, TDDFT calculations were performed on the above DFT-optimized structure in the gas phase. Their predicted absorption spectra are shown in Figure S4 in the Supporting Information, and their corresponding excitation energy, oscillator strength (*f*), and dominant contributing transitions are collected in Table S1 in the Supporting Information. Overall, *rac*-$\mathbf{2}^{2+}$ and *meso*-$\mathbf{2}^{2+}$ have very similar absorption patterns. However, the meso isomer was predicted to have relatively higher oscillator strength. The predicted HOMO → LUMO excitation at 680 nm is responsible for the observed low-energy edge around 700 nm. Two MLCT transition peaks, although overlapping with each other, could be distinguished around 560 and 490 nm for complex $\mathbf{2}^{2+}$. The former peak at 560 nm is ascribed to the MLCT transitions from HOMO−1 and HOMO−2 (S_5−S_8 for *rac*-$\mathbf{2}^{2+}$ and S_5 and S_7 for *meso*-$\mathbf{2}^{2+}$). The latter peak at 490 nm is mainly from HOMO−3 and HOMO−4 (S_{10}−S_{13} for *rac*-$\mathbf{2}^{2+}$ and S_{11} and S_{12} for *meso*-$\mathbf{2}^{2+}$). All of these occupied orbitals are dominated by the metal component (Figures S2 and S3 in the Supporting Information).

NIR Transition Analysis of Open-Shell Complexes. The large K_c value of $\mathbf{2}^{2+}$ (2.87×10^7) allows us to precisely titrate it with 1 or 2 equiv of oxidant, cerium ammonium nitrate (CAN). Corresponding visible/NIR absorption spectral changes are provided in Figure 6a,b. When a solution of $\mathbf{2}^{2+}$ in acetonitrile was gradually treated with CAN up to 1 equiv (Figure 6a), MLCT transitions decrease continually with the concomitant emergence of broad bands between 900 and 2700 nm. When the amount of CAN was gradually increased to 2 equiv, NIR transitions decrease gradually until they vanish (Figure 6b). Clearly, the new generated NIR bands after treatment with 1 equiv of CAN are associated with the one-electron-oxidized open-shell system $\mathbf{2}^{3+}$. It seems that several overlapping peaks are present in those NIR bands. Thus, they were deconvoluted into three peaks at 1059, 1283, and 1827 nm, respectively (Figure 6e), by assuming Gaussian shapes. From a comparison of the deconvoluted NIR transitions of $\mathbf{2}^{3+}$ and $\mathbf{1}^{3+}$ (Figure 6e,f), we note that those of the tris-bidentate complex $\mathbf{2}^{3+}$ are broader, weaker, and in a lower energy region than those of the bis-tridentate complex $\mathbf{1}^{3+}$. Oxidative titration experiments were also carried out on the monometallic complex $\mathbf{3}^{+}$ and $\mathbf{4}^{+}$ (Figure 6c,d), which manifested the decrease of the MLCT bands in the visible region and the emergence of ligand-to-metal charge-transfer (LMCT) transitions around 800 nm upon one-electron oxidation. It should be noted that the energies of those new LMCT bands are much higher than those of the NIR transitions of $\mathbf{1}^{3+}$ and $\mathbf{2}^{3+}$, which excludes the possibility of mixing some LMCT bands in Figure 6e,f.

NIR transitions could also be observed during oxidative spectroelectrochemical analysis of $\mathbf{1}^{2+}$ and $\mathbf{2}^{2+}$ (Figures S5−S10 in the Supporting Information). For instance, when a solution of $\mathbf{1}^{2+}$ in acetonitrile was electrolyzed by applying various potentials increasing stepwisely from +0.05 to +0.5 V vs Ag/AgCl, multiple transitions in the NIR region appeared (Figure S5 in the Supporting Information). When the potential was further increased from +0.5 to +0.8 V, these new NIR transitions went down. The shape and energy of these NIR bands in the one-electron-oxidized state ($\mathbf{1}^{3+}$) is very similar to those observed during chemical oxidation with CAN. Similar spectroelectrochemical experiments were carried out with the tris-bidentate complex $\mathbf{2}^{2+}$ and in different solvents. Figure 7 shows the absorption spectra of $\mathbf{1}^{3+}$ and $\mathbf{2}^{3+}$ recorded during spectroelectrochemical experiments in CH_3CN, CH_2Cl_2, and DMF, respectively. It is very clear that the NIR transitions of $\mathbf{1}^{3+}$ and $\mathbf{2}^{3+}$ exhibit only slight differences in the different solvents used, which means that they are virtually solvent-independent. These facts suggest than complexes $\mathbf{1}^{3+}$ and $\mathbf{2}^{3+}$ belong to a fully delocalized open-shell system.

From the above electrochemical, DFT, and spectroscopic analysis, we know that the bridging biscyclometalating ligand of **2** is redox-noninnocent like that in **1**. The observed NIR bands of $\mathbf{1}^{3+}$ and $\mathbf{2}^{3+}$ cannot be interpreted as intervalence charge-transfer (IVCT) transitions, and the classical Marcus−Hush theory is not applicable for these systems. Computational calculations on the one-electron-oxidized complex $\mathbf{2}^{3+}$ were then carried out to elucidate the nature of its electronic structure and the observed NIR transitions. DFT and TDDFT

dx.doi.org/10.1021/ic202295b | *Inorg. Chem.* 2012, 51, 1590−1598

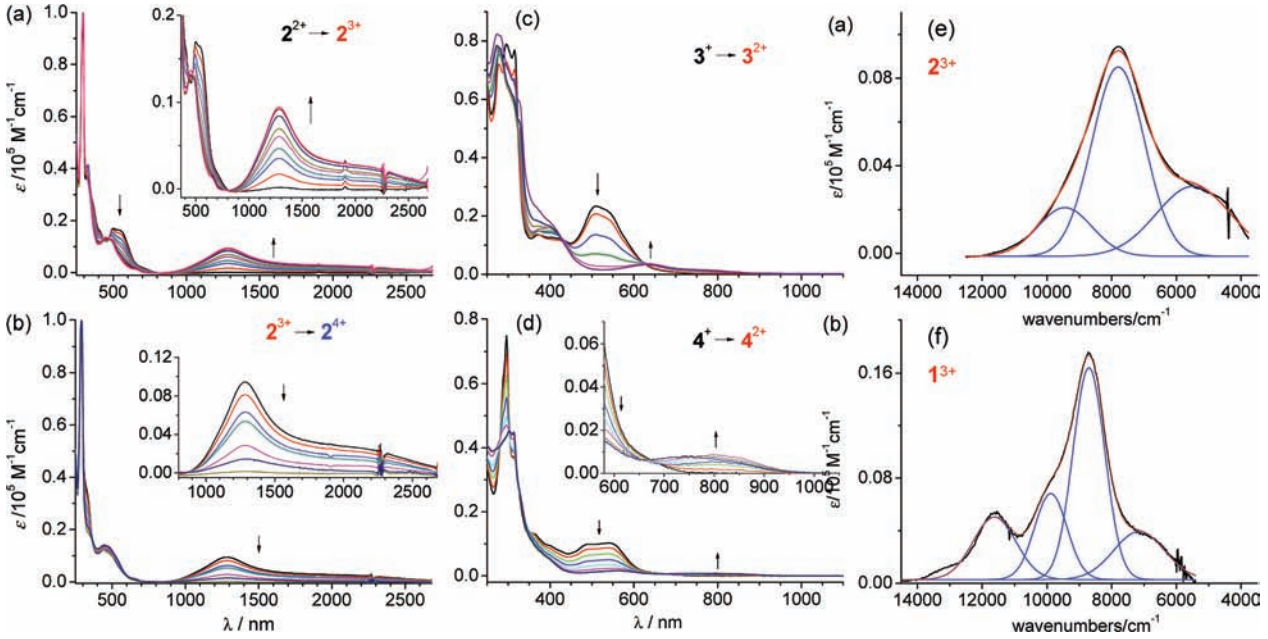

Figure 6. Absorption spectral changes of $\mathbf{2}^{2+}$ (a and b), $\mathbf{3}^{+}$ (c) and $\mathbf{4}^{+}$ (d) in acetonitrile upon one-electron (a, c, d) and two-electron (b) oxidation by adding different equivalents of CAN while keeping the concentration of complexes constant. (e) and (f) are deconvolution plots of the NIR spectra of $\mathbf{2}^{3+}$ (a) and $\mathbf{1}^{3+}$ (b) generated by adding 1 equiv CAN in acetonitrile. The black lines are experimentally observed spectra. The blue lines are individual deconvoluted peaks. The red lines are the sum of blue lines.

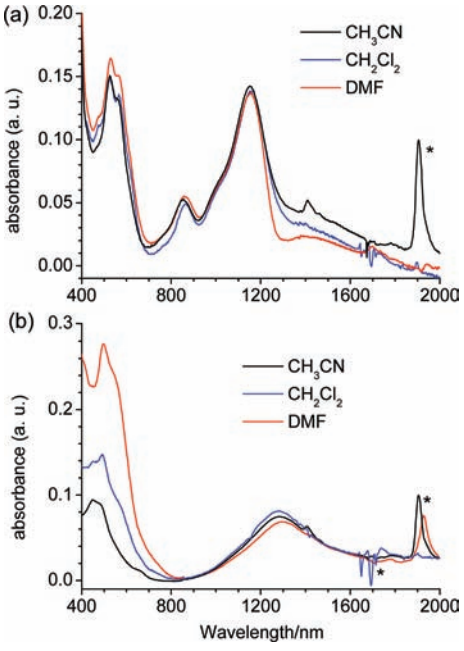

Figure 7. Absorption spectra (a) $\mathbf{1}^{3+}$ and (b) $\mathbf{2}^{3+}$ in indicated solvents (CH_3CN, CH_2Cl_2, or DMF) recorded during oxidative spectroelectrochemistry measurements.

calculations have previously been employed to interpret organometallic systems with redox-noninnocent ligands.[29] We carried out DFT calculations on both rac and meso isomers of $\mathbf{2}^{3+}$ at the UB3LYP level[30] with the effective core potential LanL2DZ basis set for ruthenium[31] and 6-31G* for other atoms in vacuo.[32] The Mulliken spin-density plots of *rac*-$\mathbf{2}^{3+}$ and *meso*-$\mathbf{2}^{3+}$, together with that of $\mathbf{1}^{3+}$, are shown in Figure 8. It is clear that the spins of these complexes are evenly distributed along the central Ru−phenyl−Ru array, which points to a strong electron delocalization in these systems. The spin-density population of these complexes is delineated in Table 2. *rac*-$\mathbf{2}^{3+}$ and *meso*-$\mathbf{2}^{3+}$ have very similar spin distributions. Ruthenium atoms have almost identical spin densities (0.385 each), which is in accordance with the electron delocalization nature of $\mathbf{2}^{3+}$. A significant portion of spin resides in the cyclometalating phenyl ring (a total of 0.251 for *rac*-$\mathbf{2}^{3+}$ and 0.249 for *meso*-$\mathbf{2}^{3+}$), with the carbon atoms directly connecting with the metal center having the highest density.

TDDFT calculations were performed on the above DFT-optimized structure of both *rac*-$\mathbf{2}^{3+}$ and *meso*- $\mathbf{2}^{3+}$ at the same UB3LYP/LanL2DZ/6-31G* level in vacuo. Calculated low-energy excitations with oscillator strengths (f) larger than 0.001 are provided in Table S2 in the Supporting Information. Corresponding spin orbitals involved in these transitions are given in Figure S11 in the Supporting Information. The predicted low-energy transitions of *rac*-$\mathbf{2}^{3+}$ and *meso*-$\mathbf{2}^{3+}$ are very similar. The major NIR absorption peak of $\mathbf{2}^{3+}$ at 1283 nm is well predicted by TDDFT results (S_5 of *rac*-$\mathbf{2}^{3+}$ and *meso*-$\mathbf{2}^{3+}$), in terms of both energy and strength. This transition is mainly associated with the excitation of a β electron from β-HOSO (highest occupied spin orbital) and β-HOSO−4 to β-LUSO (lowest unoccupied spin orbital). The experimentally observed lowest-energy peak at 1827 nm is likely associated with the S_1 and S_3 excitations, which involve excitation of a β electron to β-LUSO from β-HOSO and β-HOSO−1 for *rac*-$\mathbf{2}^{3+}$ and from β-HOSO and β-HOSO−2 for *meso*-$\mathbf{2}^{3+}$. All of these excitations could be interpreted as the charge-transfer transition from the metal centers to the biscyclometalating phenyl ring. However, the metal centers in different occupied orbitals have different orbital configurations. For instance, in the case of *rac*-$\mathbf{2}^{3+}$, β-HOSO, β-HOSO−1, and β-HOSO−4 consist of ruthenium atoms mainly with d_{xy}, d_{xz}, and d_{yz} configurations, respectively. In the case of *meso*-$\mathbf{2}^{3+}$, ruthenium atoms of β-HOSO, β-HOSO−2, and β-HOSO−4 are dominated by d_{xz}, d_{xy}, and $d_{3z^2-r^2}$, respectively. TDDFT calculations do not predict the observed shoulder band at 1059 nm. The same situation

dx.doi.org/10.1021/ic202295b | Inorg. Chem. 2012, 51, 1590−1598

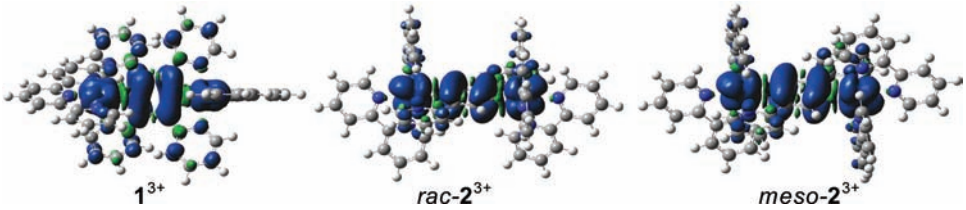

Figure 8. Spin-density plots of $\mathbf{1}^{3+}$, *rac*-$\mathbf{2}^{3+}$, and *meso*-$\mathbf{2}^{3+}$.

Table 2. Calculated Spin-Density Distributions of Complexes $\mathbf{1}^{3+}$, *rac*-$\mathbf{2}^{3+}$, and *meso*-$\mathbf{2}^{3+}$ on the Level of UB3LYP/LanL2DZ/6-31G*[a]

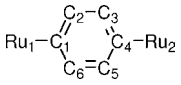

	spin density		
atom	$\mathbf{1}^{3+}$	*rac*-$\mathbf{2}^{3+}$	*meso*-$\mathbf{2}^{3+}$
Ru_1	0.326	0.384	0.385
Ru_2	0.326	0.385	0.385
C_1	0.050	0.063	0.062
C_2	0.043	0.027	0.035
C_3	0.043	0.036	0.027
C_4	0.050	0.062	0.062
C_5	0.043	0.027	0.035
C_6	0.043	0.036	0.027
phenyl	0.272	0.251	0.249

[a]The spin density is determined by the difference of the Mulliken charges of α and β electrons ($\alpha - \beta$).

was previously found for comeplx $\mathbf{1}^{3+}$.[19] We acknowledge that TDDFT results did not fully agree with the observed NIR transitions for complexes $\mathbf{1}^{3+}$ and $\mathbf{2}^{3+}$. However, their major absorption peak has been well predicted, in terms of both energy and strength. In this sense, TDDFT results provide useful and instructive information regarding the charge delocalizations of these open-shell systems.

Classical Marcus–Hush two-state theory neglects the importance of the bridging ligand in mediating electron transfer between individual redox sites, and it predicts the presence of a single IVCT band, although the band shape is dependent on the degree of electronic coupling. Considering the redox-noninnocent nature of the bridging ligand in systems $\mathbf{1}^{3+}$ and $\mathbf{2}^{3+}$ and the failure of TDDFT calculations to fully predict their NIR transitions, we turn to a three-state model[33] developed by Brunschwig, Creutz, and Sutin for the explanation of NIR transitions of $\mathbf{1}^{3+}$ and $\mathbf{2}^{3+}$. This model adopts a third bridge state beyond the donor and acceptor states. When the bridge state lies higher in energy than the other two states, the three-state model predicts the presence of two open-shell system-associated NIR transitions. The low-energy band is metal-to-metal charge transfer (MMCT) in character, and the high-energy transition is metal–bridging ligand charge transfer (MBCT). We know that oxidation of the dianionic phenyl bridge is supposed to be more difficult than the $Ru^{II/III}$ process in cyclometalated complexes. In the electrochemical analysis of some cyclometalated ruthenium complexes,[12,16,17] a second oxidation wave (mostly irreversible) beyond the $Ru^{II/III}$ process at a more positive potential is often observed and that wave is mainly associated with oxidation of the anionic ligand. In this sense, the bridge-dominated state in systems $\mathbf{1}^{3+}$ and $\mathbf{2}^{3+}$ should be higher in energy than the metal-dominated state and the three-state model is applicable to them. Thus, in $\mathbf{1}^{3+}$ and $\mathbf{2}^{3+}$, the major peaks at 1147 and 1283 nm, respectively, are assigned to MMCT bands. The nearby peaks on the higher side (1012 and 1059 nm, respectively) are attributed to MBCT bands. The peak in the lowest-energy region could be due to vibration signatures, which tend to play a more important role in fully delocalized systems. As for the small band at 860 nm in tridentate complex $\mathbf{1}^{3+}$, it is likely resulting from the red shift of the band at 805 nm before oxidation ($\mathbf{1}^{2+}$; see the oxidative titration spectral changes in Figure 5a of ref 19). We note that such a band is not present in both $\mathbf{2}^{2+}$ and $\mathbf{2}^{3+}$ with bidendate coordination. More complicated analysis using three-state models and simulation of the absorption spectra will be carried out in the near future.

Electron Paramagnetic Resonance (EPR) Studies. EPR spectroscopy is a useful tool for analyzing the spin distributions for ruthenium complexes with redox-noninnocent ligands. A free organic spin has a g factor $g_e = 2.0023$. A low-spin Ru^{III} species is usually EPR-inactive at room temperature because of rapid spin–lattice relaxation. However, it could exhibit a rhombic or axial EPR signal at low temperature as solid or frozen solutions. The anisotropy Δg ($=g_1 - g_3$) and the deviation of the isotropic g factor $\langle g \rangle$ ($=[(g_1^2 + g_2^2 + g_3^2)/3]^{1/2}$) from g_e reflects the spin distribution of the complex and symmetry at the metal center as a result of spin–orbital coupling and low-symmetry ligand-field effects.[34] The larger of the Δg value and the deviation, the higher the amount of spin is on the metal center. For example, a true metal-centered spin of a cetecholatoruthenium(III) complex has a $\langle g \rangle$ value of 2.476 with $\Delta g = 0.833$.[34a] However, complex $\mathbf{1}^{3+}$ exhibits a rhombic EPR signal at 77 K with $\langle g \rangle$ and Δg values of 2.144 and 0.34, respectively.[19] The substantially low $\langle g \rangle$ and Δg values of complex $\mathbf{1}^{3+}$ are a result of significant participation of ligand oxidation. However, the pronounced rhombicity of the EPR signal indicates that the amount of spin on the metals is more than that on the organic ligand. In comparison, complex $\mathbf{2}^{3+}$ displays an axial EPR signal at low temperature with $g_1 = g_2 = 2.106$ and $g_3 = 1.857$ (Figure 9). The $\langle g \rangle$ and Δg values are

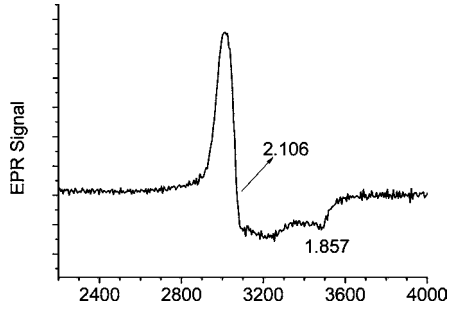

Figure 9. EPR signal of $\mathbf{2}^{3+}$ at 77 K in acetonitrile. The spectrometer frequency ν is 9.519×10^9 Hz.

calculated to be 2.026 and 0.249, which are comparable to those of $\mathbf{1}^{3+}$. Both rhombic and axial EPR signals have been documented for a variety of Ru^{III} complexes with t_{2g}^5 electronic

dx.doi.org/10.1021/ic202295b | Inorg. Chem. 2012, 51, 1590–1598

configuration.[34] Larger distortions from the octahedral field probably exist in the tridentate complex $\mathbf{1}^{3+}$ than the bidentate complex $\mathbf{2}^{3+}$, as suggested by their different g splittings. Nevertheless, low $\langle g \rangle$ and Δg values of these two complexes signify an appreciable amount of ligand participation at their singly occupied molecular orbitals, which is consistent with the presence of a redox-noninnocent bridging ligand.

CONCLUSION

To conclude, we present in this paper studies of the electronic properties of the 1,4-benzenedicyclometalated ruthenium complex with either bis-tridentate or tris-bidentate coordination mode. The electrochemical studies of the bidentate complex $[(bpy)_2Ru(dpb)Ru(bpy)_2]^{2+}$ establish that the in situ generated one-electron-oxidized complex has a relatively large comproportionation constant (2.87×10^7) in acetonitrile, which is comparable to that of the tridentate complex $[(tpy)Ru(tpb)Ru(tpy)]^{3+}$. However, the absorption spectra of $[(bpy)_2Ru(dpb)Ru(bpy)_2]^{2+}$ and $[(tpy)Ru(tpb)Ru(tpy)]^{2+}$ are significantly different. The separate and distinct low-energy band at 805 nm of the bis-tridentate complex is not present in the tris-bidentate complex. We attribute this difference to the different LUMO compositions and energy levels of these complexes. DFT calculations indicate that the bridging-ligand-associated LUMO of $[(tpy)Ru(tpb)Ru(tpy)]^{2+}$ is much more stabilized than the bpy-dominated LUMO level of $[(bpy)_2Ru(dpb)Ru(bpy)_2]^{2+}$. As a matter of fact, this difference significantly affects the electronic properties of these two complexes.

$[(bpy)_2Ru(dpb)Ru(bpy)_2]^{2+}$ could be precisely titrated with CAN to give one-electron-oxidized complex $[(bpy)_2Ru(dpb)Ru(bpy)_2]^{3+}$ and two-electron-oxidized complex $[(bpy)_2Ru(dpb)Ru(bpy)_2]^{4+}$. Alternatively, oxidative electrolysis of both complexes also generated open-shell species of these complexes and the corresponding NIR transition energy was virtually independent of the solvents used (acetonitrile, CH_2Cl_2, and DMF). TDDFT calculations suggest that the major NIR peak of $[(bpy)_2Ru(dpb)Ru(bpy)_2]^{3+}$ is associated with the charge-transfer transitions from the metal components to the biscyclometalating benzene ring. EPR studies imply that an appreciable amount of free spin is distributed on the briding ligand. These studies establish that a 1,4-benzene dianion, when covalently coupled to two ruthenium atoms with either a bis-tridentate or tris-bidentate coordination mode, behaves as a redox-noninnocent bridging ligand and the corresponding open-shell complex is a fully delocalized system across the Ru−phenyl−Ru motif. However, the bis-tridentate complex is more appealing to us, because of higher stability, linear configuration, the presence of low-energy absorption, and the separation of MMCT and MBCT bands in the NIR region. Future work will involve spectral simulation of NIR spectra using a three-state model and studies of a series of tridentate complexes with different substituents on the auxiliary tpy ligands.

EXPERIMENTAL SECTION

Spectroscopic Measurements. All optical ultraviolet/visible (UV/vis) absorption spectra were obtained using a TU-1810DSPC spectrometer of Beijing Purkinje General Instrument Co. Ltd. at room temperature in denoted solvents, with a conventional 1.0 cm quartz cell. UV/vis/NIR spectra were recorded using a PE Lambda 750 UV/vis/NIR spectrophotometer.

Electrochemical Measurements. All CV were taken using a CHI620D potentiostat. All measurements were carried out in 0.1 M of Bu_4NClO_4/acetonitrile at a scan rate of 100 mV/s with a Ag/AgCl reference electrode. The working electrode was glassy carbon, and a platinum coil was used as the counter electrode.

Oxidative Spectroelectrochemistry. Oxidative spectroelectrochemistry was performed in a thin-layer cell (optical length = 0.2 cm) in which an indium−tin oxide glass electrode was set in an indicated solvent containing $[\mathbf{1}](\mathbf{PF_6})_2$ or $[\mathbf{2}](\mathbf{PF_6})_2$ (the concentration is around 1×10^{-4} M) and 0.1 M TBAP as the supporting electrolyte. A platinum wire and Ag/AgCl in a saturated aqueous solution were used as the counter and reference electrodes, respectively. The cell was put into a PE Lambda 750 UV/vis/NIR spectrophotometer to monitor spectral changes during electrolysis.

Computational Methods. DFT calculations were carried out using the B3LYP exchange correlation functional[30] and implemented in the *Gaussian 03* program package.[35] The electronic structures of the complexes were determined using a general basis set with the Los Alamos effective core potential LanL2DZ basis set for ruthenium[31] and 6-31G* for other atoms in vacuo.[32]

Synthesis. NMR spectra were recorded in the designated solvent on a Bruker Avance 400 MHz spectrometer. Spectra are reported in ppm values from residual protons of the deuterated solvent for ^{1}H NMR (7.26 ppm for $CDCl_3$ and 1.92 ppm for CD_3CN) and ^{13}C NMR (77.00 ppm for $CDCl_3$). MS data were obtained with a Bruker Daltonics Inc. Apex II FT-ICR or Autoflex III MALDI-TOF mass spectrometer. The matrix for matrix-assisted laser desorption ionization time-of-flight (MALDI-TOF) measurement is α-cyano-4-hydroxycinnamic acid. Microanalysis was carried out using a Flash EA 1112 or Carlo Erba 1106 analyzer at the Institute of Chemistry, Chinese Academy of Sciences.

Synthesis of 5. To 50 mL of degassed toluene were added 1,4-dibromobenzene (566 mg, 2.4 mmol), 2-pyridyltributylstannane (4.4 g, 12 mmol), $Pd(PPh_3)Cl_2$ (224 mg, 0.32 mmol), and LiCl (1.0 g, 24 mmol). After bubbling with nitrogen, the system was refluxed in a sealed pressure tube for 4 days. The mixture was concentrated and subjected to flash column chromatography on silica gel to afford 390.8 mg of **5** in a yield of 70% (eluent: 6:1 petroleum ether/ethyl acetate). ^{1}H NMR (400 MHz, $CDCl_3$): δ 7.25 (m, 2H), 7.77 (m, 4H), 8.14 (s, 4H), 7.72 (d, J = 4.2 Hz, 2H). ^{13}C NMR (100 MHz, $CDCl_3$): δ 120.6, 122.3, 127.2, 127.3, 136.7, 139.7, 149.7, 156.8. EI-MS: 232 for $[M]^+$.

Synthesis of $[\mathbf{4}](\mathbf{PF_6})$ and $[\mathbf{2}](\mathbf{PF_6})_2$. To 10 mL of dry acetone were added $Ru(bpy)_2Cl_2 \cdot 2H_2O$ (104 mg, 0.2 mmol) and AgOTf (154 mg, 0.6 mmol), and the system was refluxed for 3 h before cooling to room temperature. The mixture was filtered to remove unwanted precipitates, and the filtrate was concentrated to dryness. To the residue were added ligand **5** (23 mg, 0.1 mmol), DMF (10 mL), and ^{t}BuOH (10 mL), and the mixture was refluxed in a sealed pressure tube for 48 h. After cooling to room temperature, the solvent was removed under reduced pressure, and the residue was dissolved in the proper amount of methanol. After the addition of an excess of KPF_6, the resulting precipitate was collected by filtering and washing with water and Et_2O. The obtained solid was subjected to flash column chromatography on neutral Al_2O_3 (eluent: 50:1 → 10:1 → 2:1 CH_2Cl_2/CH_3CN) to give 31 mg of complex $[\mathbf{4}](\mathbf{PF_6})$ (40%) and 24 mg of complex $[\mathbf{2}](\mathbf{PF_6})_2$ (18%). Characterization data for $[\mathbf{4}](\mathbf{PF_6})$. ^{1}H NMR (400 MHz, CD_3CN): δ 6.95 (t, J = 6.3 Hz, 1H), 7.04 (s, 1H), 7.16−7.26 (m, 4H), 7.42 (m, 2H), 7.56 (d, J = 8.2 Hz, 1H), 7.59 (d, J = 5.6 Hz, 1H), 7.66 (t, J = 7.8 Hz, 1H), 7.71 (t, J = 7.8 Hz, 1H), 7.76−7.87 (m, 6H), 7.93 (d, J = 8.2 Hz, 1H), 7.99 (t, J = 7.8 Hz, 1H), 8.08 (d, J = 8.2 Hz, 1H), 8.13 (d, J = 5.5 Hz, 1H), 8.30 (d, J = 8.2 Hz, 1H), 8.34 (d, J = 8.2 Hz, 1H), 8.39 (d, J = 8.2 Hz, 1H), 8.46 (d, J = 8.2 Hz, 1H), 8.49 (d, J = 4.6 Hz, 1H). MALDI-MS: 645.3 for $[M - PF_6]^+$. Anal. Calcd for $C_{36}H_{27}N_6RuPF_6 \cdot H_2O$: C, 53.53; H, 3.62; N, 10.41. Found: C, 53.57; H, 3.48; N, 10.27. Characterization data for $[\mathbf{2}](\mathbf{PF_6})_2$. MALDI-MS: 1202.4 for $[M - PF_6]^+$. Anal. Calcd for $C_{56}H_{42}N_{10}Ru_2P_2F_{12} \cdot 3H_2O$: C, 48.00; H, 3.45; N, 10.00. Found: C, 47.82; H, 3.16; N, 9.93.

ASSOCIATED CONTENT

Supporting Information

DFT-optimized structures of rac and meso diastereomers of $\mathbf{2}^{2+}$, selected frontier molecular orbital graphics of $\mathbf{2}^{2+}$, simulation of absorption spectra of $\mathbf{2}^{2+}$, oxidative spectroelectrochemistry

of $\mathbf{1}^{2+}$ and $\mathbf{2}^{2+}$, calculated low-energy excitations of *rac*-$\mathbf{2}^{3+}$ and *meso*-$\mathbf{2}^{3+}$ and involved frontier spin orbitals, and NMR and MS spectra of new compounds. This material is available free of charge via the Internet at http://pubs.acs.org.

AUTHOR INFORMATION

Corresponding Author

*E-mail: zhongyuwu@iccas.ac.cn.

Author Contributions

[§]These authors contributed equally.

ACKNOWLEDGMENTS

Y.-W.Z. thanks the National Natural Science Foundation of China (Grant 21002104), the National Basic Research 973 program of China (Grant 2011CB932301), the Scientific Research Foundation for the Returned Overseas Chinese Scholars, State Education Ministry of China, and the Institute of Chemistry, Chinese Academy of Sciences ("100 Talent" Program), for financial support.

REFERENCES

(1) (a) Albrecht, M. *Chem. Rev.* **2010**, *110*, 576. (b) Djukic, J.-P.; Sortais, J.-B.; Barloy, L.; Pfeffer, M. *Eur. J. Inorg. Chem.* **2009**, 817. (c) Chi, Y.; Chou, P.-T. *Chem. Soc. Rev.* **2010**, *39*, 638. (d) Paul, F.; Lapinte, C. *Coord. Chem. Rev.* **1998**, *178*, 431.

(2) (a) Long, N. J.; Williams, C. K. *Angew. Chem., Int. Ed.* **2003**, *42*, 2586. (b) Ren, T. *Organometallics* **2005**, *24*, 4854. (c) Low, P. J.; Roberts, R. L.; Cordiner, R. L.; Hartl, F. *J. Solid State Electrochem.* **2005**, *9*, 717.

(3) (a) Mücke, P.; Linseis, M.; Záliš, S.; Winter, R. F. *Inorg. Chim. Acta* **2011**, *374*, 36. (b) Maurer, J.; Linseis, M.; Sarkar, B.; Schwederski, B.; Niemeyer, M.; Kaim, W.; Záliš, S.; Anson, C.; Zabel, M.; Winter, R. F. *J. Am. Chem. Soc.* **2008**, *130*, 259. (c) Li, F.; Cheng, J.; Chai, X.; Jin, S.; Wu, X.; Yu, G.-A.; Liu, S. H.; Chen, G. Z. *Organometallics* **2011**, *30*, 1830.

(4) (a) Duati, M.; Tasca, S.; Lynch, F. C.; Bohlen, H.; Vos, J. G.; Stagni, S.; Ward, M. D. *Inorg. Chem.* **2003**, *42*, 8377. (b) Duati, M.; Fanni, S.; Vos, J. G. *Inorg. Chem. Commun.* **2000**, *3*, 68.

(5) (a) Koutsantonis, G. A.; Jenkins, G. I.; Schauer, P. A.; Szczepaniak, B.; Skelton, B. W.; Tan, C.; White, A. H. *Organometallics* **2009**, *28*, 2195. (b) Wong, C.-Y.; Lai, L.-M.; Pat, P.-K. *Organometallics* **2009**, *28*, 5656. (c) Khairul, W. M.; Fox, M. A.; Schauer, P. A.; Albesa-Jové, D.; Yufit, D. S.; Howard, J. A. K.; Low, P. J. *Inorg. Chim. Acta* **2011**, *374*, 461. (d) Olivier, C.; Costuas, K.; Choua, S.; Maurel, V.; Turek, P.; Saillard, J.-Y.; Touchard, D.; Rigaut, S. *J. Am. Chem. Soc.* **2010**, *132*, 5638. (e) Pevny, F.; Piazza, E. D.; Norel, L.; Drescher, M.; Winter, R. F.; Rigaut, S. *Organometallics* **2010**, *29*, 5912. (f) Wu, X.-H.; Liang, J. H.; Xia, J.-L.; Jin, S.; Yu, G.-A.; Liu, S. H. *Organometallics* **2010**, *29*, 1150. (g) Yang, W.-W.; Wang, L.; Zhong, Y.-W.; Yao, J. *Organometallics* **2011**, *30*, 2236. (h) Zhong, Y.-W.; Wu, S.-H.; Burkhardt, S. E.; Yao, C.-J.; Abruña, H. D. *Inorg. Chem.* **2011**, *50*, 517. (i) Yang, W.-W.; Zhong, Y.-W.; Yoshikawa, S.; Shao, J.-Y.; Masaoka, S.; Sakai, K.; Yao, J.; Haga, M.-a. *Inorg. Chem.* DOI: 10.1021/ic2016885.

(6) (a) Cao, Z.; Forrest, W. P.; Gao, Y.; Fanwick, P. E.; Zhang, Y.; Ren, T. *Inorg. Chem.* **2011**, *50*, 7364. (b) Ghazala, S. I.; Paul, F.; Toupet, L.; Roisnel, T.; Hapiot, P.; Lapinte, C. *J. Am. Chem. Soc.* **2006**, *128*, 2463.

(7) (a) Bellows, D.; Goudreault, T.; Aly, S. M.; Fortin, D.; Gros, C. P.; Barbe, J.-M.; Harvey, P. D. *Organometallics* **2010**, *29*, 317. (b) McGuire, R. Jr.; McGuire, M. C.; McMillin, D. R. *Coord. Chem. Rev.* **2010**, *254*, 2574. (c) Ni, J.; Zhang, X.; Wu, Y.-H.; Zhang, L.-Y.; Chen, Z.-N. *Chem.—Eur. J.* **2011**, *17*, 1171. (d) Wu, S.-H.; Burkhardt, S. E.; Yao, J.; Zhong, Y.-W.; Abruña, H. D. *Inorg. Chem.* **2011**, *50*, 3959.

(8) You, Y.; Park, S. Y. *Dalton Trans.* **2009**, 1267.

(9) (a) Li, J.; Siegler, M.; Lutz, M.; Spek, A. L.; Gebbink, R. J. M. K.; van Koten, G. *Adv. Synth. Catal.* **2010**, *352*, 2474. (b) van der Boom, M. E.; Milstein, D. *Chem. Rev.* **2003**, *103*, 1759.

(10) (a) Keller, J. M.; Glusac, K. D.; Danilov, E. O.; McIlroy, S.; Sreearuothai, P.; Cook, A. R.; Jiang, H.; Miller, J. R.; Schanze, K. S. *J. Am. Chem. Soc.* **2011**, *133*, 11289. (b) Mahapatro, A. K.; Ying, J.; Ren, T.; Janes, D. B. *Nano Lett.* **2008**, *8*, 2181.

(11) (a) Yuan, P.; Yin, J.; Yu, G.-A.; Hu, Q.; Liu, S. H. *Organometallics* **2007**, *26*, 196. (b) Bella, S. D. *Chem. Soc. Rev.* **2001**, *30*, 355.

(12) (a) Bomben, P. G.; Koivisto, B. D.; Berlinguette, C. P. *Inorg. Chem.* **2010**, *49*, 4960. (b) Koivisto, B. D.; Robson, K. C. D.; Berlinguette, C. P. *Inorg. Chem.* **2009**, *48*, 9644. (c) Robson, K. C. D.; Koivisto, B. D.; Yella, A.; Sporinova, B.; Nazeeruddin, M. K.; Baumgartner, T.; Gratzel, M.; Berlinguette, C. P. *Inorg. Chem.* **2011**, *50*, 5494.

(13) (a) Ward, M. D.; McCleverty, J. A. *J. Chem. Soc., Dalton Trans.* **2002**, 275. (b) Boyer, J. L.; Rochford, J.; Tsai, M.-K.; Muckerman, J. T.; Fujita, E. *Coord. Chem. Rev.* **2010**, *254*, 309. (c) Lever, A. B. P. *Coord. Chem. Rev.* **2010**, *254*, 1397. (d) Lever, A. B. P.; Gorelsky, S. I. *Struct. Bonding (Berlin)* **2004**, *107*, 77. (e) Dzik, W. I.; van der Vlugt, J. I.; Reek, J. N. H.; de Bruin, B. *Angew. Chem., Int. Ed.* **2011**, *50*, 3356.

(14) (a) Keller, J. M.; Schanze, K. S. *Organometallics* **2009**, *28*, 4210. (b) Gao, L.-B.; Kan, J.; Fan, Y.; Zhang, L.-Y.; Liu, S.-H.; Chen, Z.-N. *Inorg. Chem.* **2007**, *46*, 5651. (c) Fitzgerald, E. C.; Ladjarafi, A.; Brown, N. J.; Collison, D.; Costuas, K.; Edge, R.; Halet, J.-F.; Justaud, F.; Low, P. J.; Meghezzi, H.; Roisnel, T.; Whiteley, M. W.; Lapinte, C. *Organometallics* **2011**, *30*, 4180.

(15) Man, W. Y.; Xia, J.-L.; Brown, N. J.; Farmer, J. D.; Yufit, D. S.; Howard, J. A. K.; Liu, S. H.; Low, P. J. *Organometallics* **2011**, *30*, 1852.

(16) (a) Fraysse, S.; Coudret, C.; Launay, J.-P. *J. Am. Chem. Soc.* **2003**, *125*, 5880. (b) Sutter, J.-P.; Grove, D. M.; Beley, M.; Collin, J.-P.; Veldman, N.; Spek, A. L.; Sauvage, J.-P.; van Koten, G. *Angew. Chem., Int. Ed.* **1994**, *33*, 1282. (c) Steenwinkel, P.; Grove, D. M.; Veldman, N.; Spek, A. L.; van Koten, G. *Organometallics* **1998**, *17*, 5647. (d) Gagliardo, M.; Amijs, C. H. M.; Lutz, M.; Spek, A. L.; Havenith, R. W. A.; Hartl, F.; van Klink, G. P. M.; van Koten, G. *Inorg. Chem.* **2007**, *46*, 11133.

(17) (a) Yao, C.-J.; Sui, L.-Z.; Xie, H.-Y.; Xiao, W.-J.; Zhong, Y.-W.; Yao, J. *Inorg. Chem.* **2010**, *49*, 8347. (b) Wang, L.; Yang, W.-W.; Zheng, R.-H.; Shi, Q.; Zhong, Y.-W.; Yao, J. *Inorg. Chem.* **2011**, *50*, 7074.

(18) (a) Hush, N. S. *Prog. Inorg. Chem.* **1967**, *8*, 391. (b) Hush, N. S. *Electrochim. Acta* **1968**, 1005.

(19) (a) Yao, C.-J.; Zhong, Y.-W.; Yao, J. *J. Am. Chem. Soc.* **2011**, *133*, 15697. (b) Yao, C.-J.; Zhong, Y.-W.; Nie, H.-J.; Abruña, H. D.; Yao, J. *J. Am. Chem. Soc.* **2011**, *133*, 20720.

(20) Juris, A.; Balzani, V.; Barigelletti, F.; Campagna, S.; Belser, P.; Von Zelewsky, A. *Coord. Chem. Rev.* **1988**, *84*, 85.

(21) Constable, E. C. *Chem. Soc. Rev.* **2007**, *36*, 246.

(22) Bomben, P. G.; Robson, K. C.; Sedach, P. A.; Berlinguette, C. P. *Inorg. Chem.* **2009**, *48*, 9631.

(23) (a) Kaim, W.; Sarkar, B. *Coord. Chem. Rev.* **2007**, *251*, 584. (b) D'Alessandro, D. M.; Keene, F. R. *Pure Appl. Chem.* **2008**, *80*, 1.

(24) Fujita, M.; Oka, H.; Ogura, K. *Tetrahedron Lett.* **1995**, *36*, 5247.

(25) Tsuboyama, A.; Takiguchi, T.; Okada, S.; Osawa, M.; Hoshino, M.; Ueno, K. *Dalton Trans.* **2004**, 1115.

(26) Ishida, N.; Moriya, T.; Goya, T.; Murakami, M. *J. Org. Chem.* **2010**, *75*, 8709.

(27) (a) Ahmed, H. M. Y.; Coburn, N.; Dini, D.; de Jong, J. J. D.; Villani, C.; Browne, W. R.; Vos, J. G. *Inorg. Chem.* **2011**, *50*, 5861. (b) Slater, J. W.; D'Alessandro, D. M.; Keene, F. R.; Steel, P. J. *Dalton Trans.* **2006**, 1954. (c) MacDonnell, F. M.; Kim, M.-J.; Wouters, K. L.; Konduri, R. *Coord. Chem. Rev.* **2003**, *242*, 47.

(28) (a) D'Alessandro, D. M.; Keene, F. R. *Dalton Trans.* **2004**, 3950. (b) Evans, D. H. *Chem. Rev.* **2008**, *108*, 2113. (c) Geiger, W. E.; Barrière, F. *Acc. Chem. Res.* **2010**, *43*, 1030.

(29) (a) Maurer, J.; Winter, R. F.; Sarkar, B.; Fiedler, J.; Záliš, S. *Chem. Commun.* **2004**, 1900. (b) Kowalski, K.; Linseis, M.; Winter,

R. F.; Zabel, M.; Záliš, S.; Kelm, H.; Krüger, H.-J.; Sarkar, B.; Kaim, W. *Organometallics* **2009**, *28*, 4196. (c) Agarwala, H.; Das, D.; Mobin, S. M.; Mondal, T. K.; Lahiri, G. K. *Inorg. Chim. Acta* **2011**, *374*, 216.
(30) (a) Lee, C.; Yang, W.; Parr, R. G. *Phys. Rev. B* **1988**, *37*, 785. (b) Becke, A. D. *J. Chem. Phys.* **1993**, *98*, 5648.
(31) (a) Hay, P. J.; Wadt, W. R. *J. Chem. Phys.* **1985**, *82*, 270. (b) Wadt, W. R.; Hay, P. J. *J. Chem. Phys.* **1985**, *82*, 284. (c) Hay, P. J.; Wadt, W. R. *J. Chem. Phys.* **1985**, *82*, 299.
(32) (a) Dunning, T. H.; Hay, P. J. In *Modern Theoretical Chemistry*; Schaefer, H. F., Ed.; Plenum: New York, 1976; Vol. 3, p 1. (b) Hehre, W. J.; Radom, L.; Schleyer, P. V. R.; Pople, J. A. *Ab Initio Molecular Orbital Theory*; John Wiley & Sons: New York, 1986.
(33) (a) D'Alessandro, D. M.; Keene, F. R. *Chem. Soc. Rev.* **2006**, *35*, 424. (b) Brunschwig, B. S.; Creutz, C.; Sutin, N. *Chem. Soc. Rev.* **2002**, *31*, 168. (c) Glover, S. D.; Kubiak, C. P. *J. Am. Chem. Soc.* **2011**, *133*, 8721. (d) Launay, J.-P.; Coudret, C.; Hortholary, C. *J. Phys. Chem. B* **2007**, *111*, 6788. We thank the reviewer for bringing this to our attention and giving constructive comments.
(34) (a) Patra, S.; Sarkar, B.; Mobin, S. M.; Kaim, W.; Lahiri, G. K. *Inorg. Chem.* **2003**, *42*, 6469. (b) Mahapatra, A. K.; Datta, S.; Goswami, S.; Mukherjee, M.; Mukherjee, A. K.; Chakravorty, A. *Inorg. Chem.* **1986**, *25*, 1715. (c) Munshi, P.; Samanta, R.; Lahiri, G. K. *J. Organomet. Chem.* **1999**, *586*, 176. (d) Kannan, S.; Kumar, K. N.; Ramesh, R. *Polyhedron* **2008**, *27*, 701.
(35) Frisch, M. J.; Trucks, G. W.; Schlegel, H. B.; Scuseria, G. E.; Robb, M. A.; Cheeseman, J. R.; Montgomery, J. A., Jr.; Vreven, T.; Kudin, K. N.; Burant, J. C.; Millam, J. M.; Iyengar, S. S.; Tomasi, J.; Barone, V.; Mennucci, B.; Cossi, M.; Scalmani, G.; Rega, N.; Petersson, G. A.; Nakatsuji, H.; Hada, M.; Ehara, M.; Toyota, K.; Fukuda, R.; Hasegawa, J.; Ishida, M.; Nakajima, T.; Honda, Y.; Kitao, O.; Nakai, H.; Klene, M.; Li, X.; Knox, J. E.; Hratchian, H. P.; Cross, J. B.; Adamo, C.; Jaramillo, J.; Gomperts, R.; Stratmann, R. E.; Yazyev, O.; Austin, A. J.; Cammi, R.; Pomelli, C.; Ochterski, J. W.; Ayala, P. Y.; Morokuma, K.; Voth, G. A.; Salvador, P.; Dannenberg, J. J.; Zakrzewski, V. G.; Dapprich, S.; Daniels, A. D.; Strain, M. C.; Farkas, O.; Malick, D. K.; Rabuck, A. D.; Raghavachari, K.; Foresman, J. B.; Ortiz, J. V.; Cui, Q.; Baboul, A. G.; Clifford, S.; Cioslowski, J.; Stefanov, B. B.; Liu, G.; Liashenko, A.; Piskorz, P.; Komaromi, I.; Martin, R. L.; Fox, D. J.; Keith, T.; Al-Laham, M. A.; Peng, C. Y.; Nanayakkara, A.; Challacombe, M.; Gill, P. M. W.; Johnson, B.; Chen, W.; Wong, M. W.; Gonzalez, C.; Pople, J. A. *Gaussian 03*, revision E.01; Gaussian Inc.: Pittsburgh, PA, 2007.